Out-of-plane electric polarization in double-fan magnetic phase of Y-type hexaferrite

Yuma Umimoto [1], Nobuyuki Abe,[1] Shojiro Kimura,[2] Yusuke Tokunaga,[1] and Taka-hisa Arima[1]

[1]*Department of Advanced Materials Science, University of Tokyo, Kashiwa 277-8561, Japan*
[2]*Institute for Materials Research, Tohoku University, Sendai 980-8577, Japan*

It has been revealed that a Y-type hexaferrite $BaSrCo_2Fe_{11.1}Al_{0.9}O_{22}$ hosts not only an in-plane (P_{ab}) but also an out-of-plane (P_c) component of magnetically induced electric polarization in the double-fan magnetic phase. With an increasing in-plane magnetic field, the magnitude of P_c reaches a maximum at around 2 T and decreases as approaching the critical field (3.8 T) of the transition to the collinear ferrimagnetic phase. P_c has also been verified to show a $120°$-period oscillation as a function of the in-plane magnetic field direction. These results are reproduced by a model combining the inverse Dzyaloshinskii-Moriya interaction and the spin-dependent pd hybridization mechanisms.

A directional filter is one of the possible applications of magnetoelectric (ME) coupling between electric polarization $\boldsymbol{P}$ and magnetization $\boldsymbol{M}$. In the view of symmetry, a ferroic order of the cross product $\boldsymbol{P} \times \boldsymbol{M}$ can be coupled with a scalar current such as light, microwave, and electric current. In experiments, it has been confirmed that the absorption coefficient of light depends on whether it propagates parallel or antiparallel to $\boldsymbol{P} \times \boldsymbol{M}$ [1–5]. Similar propagation-direction-dependent absorption of microwaves was observed in a Y-type hexaferrite $Ba_2Mg_2Fe_{12}O_{22}$ [6] owing to its antisymmetric ME tensor [7–10] forming the ferroic order of $\boldsymbol{P} \times \boldsymbol{M}$.

Hexaferrites are iron-based oxides with a hexagonal or rhombohedral lattice, and classified into M, U, W, X, Y, and Z types depending on the number and order of stacking layers in a unit cell [11,12]. U-, X-, and Y-type (M-, W-, and Z-type) hexaferrites belong to the space group $R\bar{3}m$ ($P6_3/mmc$) [11,13]. ME effects in M- [14], U- [13], Y- [7], and Z-type [15] hexaferrites have been reported in relation with the formation of a transverse-cone magnetic structure, which is known to be polar [16]. We focus on a Y-type hexaferrite $BaSrCo_2Fe_{11.1}Al_{0.9}O_{22}$, exhibiting the ME effect in a wide range of temperature [17].

Figure 1(a) shows a unit cell of $BaSrCo_2Fe_{11.1}Al_{0.9}O_{22}$ with the hexagonal basis [17,18]. Many magnetic ions included in the unit cell prevent us from determining their magnetic structures in detail. Efforts were devoted to express them in a simpler way [19–21]. It has led to a block (bunch) approximation [21] as follows. The hexagonal unit cell is divided into two types (L and S) of blocks and all the magnetic moments in each block are assumed to be ferrimagnetically aligned. Each L (S) block has a net magnetic moment $\boldsymbol{\mu}_L$ ($\boldsymbol{\mu}_S$). Rather flexible arrangements of $\boldsymbol{\mu}_L$ and $\boldsymbol{\mu}_S$ allow a variety of magnetic structures, some of which are shown in Figs. 1(b)–1(e) [22–25]. Successive phase transitions from the alternating longitudinal cone (ALC) to the double fan (DF) and finally to the collinear ferrimagnet (CFi) are induced by increasing a magnetic field perpendicular to the c axis (in-plane magnetic field) [22].

The DF magnetic structure consists of collinear ferrimagnetic (parallel to $\boldsymbol{M}$) and commensurate cycloidal (perpendicular to $\boldsymbol{M}$) components propagating along the c axis. In the latter, $\boldsymbol{\mu}_L$ and $\boldsymbol{\mu}_S$ have phases shifted by $\pm\pi/2$. The sign corresponds to the sense of the cycloidal component and we hereafter call it just the sense of the DF. The DF induces electric polarization perpendicular to both $\boldsymbol{M}$ and the c axis (in-plane component P_{ab} of electric polarization) [7–10], as expected by the spin-current [26] or the inverse Dzyaloshinskii-Moriya (DM) interaction [27] mechanism. The mechanisms expect a one-to-one correspondence between the direction of P_{ab} and the sense of the DF. On the other hand, the CFi structure produces no electric polarization.

Recently, an out-of-plane component P_c of electric polarization was found experimentally in the ALC phase [25]. It was proposed that $\boldsymbol{\mu}_L$ and $\boldsymbol{\mu}_S$ should be arranged to form an ALC structure, as shown in Fig. 1(c), where the c components of $\boldsymbol{\mu}_L$ and $\boldsymbol{\mu}_S$ are aligned in the sequence of ↑-↑-↓-↓ and the exchange striction mechanism is expected to induce P_c. This magnetic structure is hereafter called ALC-II to distinguish it from the conventional ALC-I shown in Fig. 1(b). P_c in the ALC-II phase should be independent of the direction of the helical component of the ALC structure.

We note that P_c is also expected to be allowed in the DF phase from the viewpoint of symmetry. Its direction should be determined by the sense of the DF or the direction of P_{ab}. The DF magnetic order must break all three crystalline twofold rotation axes, namely, [100], [010], and [110] axes to induce P_c. One of the twofold axes is preserved and P_c is forbidden when $\boldsymbol{M}$ is perpendicular to the crystalline twofold axis. It is because the DF is symmetric for the twofold rotation about the axis normal to both $\boldsymbol{M}$ and the c axis followed by the time-reversal operation, as shown by $2'_{\perp\boldsymbol{M}}$ in Fig. 1(e). In contrast, all of the twofold rotation symmetries are broken and P_c can be induced with $\boldsymbol{M}$ oriented along one of the twofold axes, since the twofold rotation of the DF about the axis parallel to $\boldsymbol{M}$ switches sense and is not a symmetric operation [$2_{\|\boldsymbol{M}}$ in Fig. 1(e)]. P_c should be kept by the $120°$ rotation of the DF about the c axis because of the crystalline threefold
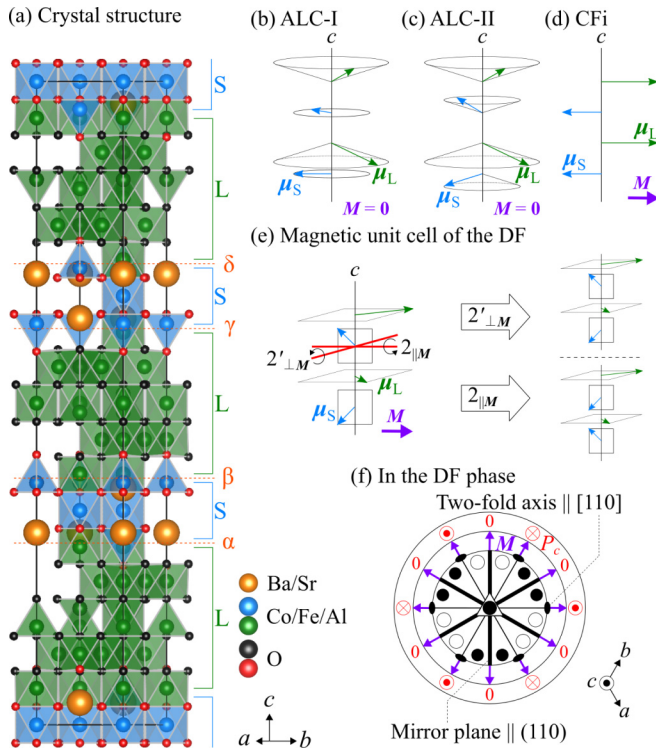
FIG. 1. (a) Crystalline unit cell of $BaSrCo_2Fe_{11.1}Al_{0.9}O_{22}$ with the hexagonal basis [17,18] drawn by VESTA [29]. Orange dashed lines express the boundaries between the L and S blocks, and red spheres denote oxygen ions on the boundaries. (b)–(e) Schematics of magnetic structures of Y-type hexaferrites within the block approximation, where the net magnetic moments μ_L and μ_S form magnetization M: (b), (c) Alternating longitudinal cone without and with the c components of μ_S (referred to as ALC-I and ALC-II, respectively), (d) collinear ferrimagnet (CFi), and (e) double fan (DF). (e) also indicates twofold rotations $2'_{\perp M}$ and $2_{\parallel M}$ of the DF about the axes (red bars) perpendicular to both M and the c axis, and parallel to M, respectively. Only the former is followed by the time reversal. (f) Relation between the directions of M (middle, purple) and the expected P_c (outer, red) in the DF phase. The crystallographic symmetries are expressed by the stereogram (center, black).

symmetry. On the other hand, P_c should be reversed when the DF is rotated by $180°$ about the c axis, because this rotation is equivalent to the space inversion about the center of the L block followed by the time reversal. The relation between the directions of M and the expected P_c is summarized in Fig. 1(f). P_c should be flipped also when the sense of the DF is switched without a change in the M direction, since it is equivalent to $2_{\parallel M}$. In this Rapid Communication, we perform an experimental study on P_c in the DF magnetic phase of $BaSrCo_2Fe_{11.1}Al_{0.9}O_{22}$. We find that the experimental results cannot be explained by any of the three known ME mechanisms, exchange striction, inverse DM, and spin-dependent pd hybridization [28], alone, but by combining the latter two mechanisms.

Single crystals of $BaSrCo_2Fe_{11.1}Al_{0.9}O_{22}$ of a nominal composition were grown by the floating-zone method [22]. The starting materials were $BaCO_3$, $SrCO_3$, Co_3O_4, Fe_2O_3, and Al_2O_3. They were mixed with the stoichiometric cation

ratio and calcined at $1100\,°C$ in air for 4 h. The reaction products were ground and pressed by a hydrostatic pressure of 24 MPa to form a rod. It was heated at $1200\,°C$ in air for 18 h. The sintered rod was cut into feed and seed rods. A molten zone was formed between them, and transferred with a speed of approximately 1 mm/h under 10 atm of oxygen gas to grow single crystals with the use of a floating-zone furnace (type D, Cannon Machinery).

For the electric and magnetic measurements, crystalline axes of the sample pieces were determined by the back-reflection Laue method. Isothermal magnetization along the [110] axis at 100 K was measured by using a superconducting quantum interference device (MPMS3, Quantum Design). In order to measure P_{ab} and P_c, two thin samples were prepared with wide surface planes perpendicular to the $[\bar{1}10]$ and [001] axes, respectively. Silver-paste electrodes were formed on the planes. The former (latter) sample had a surface area of $1.0\,mm^2$ ($2.2\,mm^2$) and thickness of 96 μm (49 μm). The sample was placed in a cryostat equipped with a super-conducting magnet. The sense of the DF was aligned by a poling electric field E_p before measuring the magnetic field dependence of P_{ab} and P_c as follows. E_p of $+2.1$ MV/m (±4.1 MV/m) was applied parallel to the $[\bar{1}10]$ ([001]) axis with a magnetic field B of $+6$ T along the [110] axis forming the CFi structure at 100 K. Next, B was reduced to $+0.3$ T to induce the transition to the DF. Then, E_p was removed. After a relaxation time longer than 30 min, the displacement current was measured by using an electrometer (6517A, Keithley) while sweeping B at 100 K without any electric field. P_{ab} and P_c were calculated by integrating the displacement current with respect to time. Here, their values were offset so that their mean values were zero in B higher than 5 T, where the nonpolar CFi structure should be dominant. The [001] sample was also used for measuring displacement current I_c along the c axis as a function of the magnetic field direction. E_p of $+4.1$ MV/m was applied along the [001] axis during reduction of B from 6 to 1.6 T in the [110] direction at 100 K, and then E_p was turned off. After 75-min relaxation, I_c was measured by using an electrometer (6517B, Keithley) while rotating the sample at a constant rate of $\pm0.58°/s$ by using a stepping motor in B of 1.6 T at 100 K without any electric field.

The isothermal magnetization M is shown in Fig. 2(a). The field derivative dM/dB shows steep changes between $+(-)2.7$ T and $+(-)3.8$ T, and M is almost flat in B higher than 3.8 T. Since the behavior is similar to a previous report [22], we assign the boundaries between the DF and the CFi phases to ±3.8 T.

Figure 2(b) shows P_{ab} and P_c as functions of B. P_{ab} decreases monotonically in increasing B. In contrast, P_c takes maxima at around ±2 T. The difference ensures that the measured P_c is not just a projection of P_{ab} resulting from experimental misalignment. P_c is expected to be coupled with the sense of the DF and hence P_{ab}, since P_c is aligned parallel to E_p. Both P_{ab} and P_c change their sign upon B reversal, which is also consistent with the expectation. P_c is suppressed for $E_p = 0$, probably because P_c's induced in DF domains with opposite senses cancel each other. Experimental results of $BaSrCo_2Fe_{11.1}Al_{0.9}O_{22}$ at 10 and 200 K and those of $Ba_{0.5}Sr_{1.5}Co_2Fe_{11.1}Al_{0.9}O_{22}$ at 100 K are shown in the Supplemental Material [30].
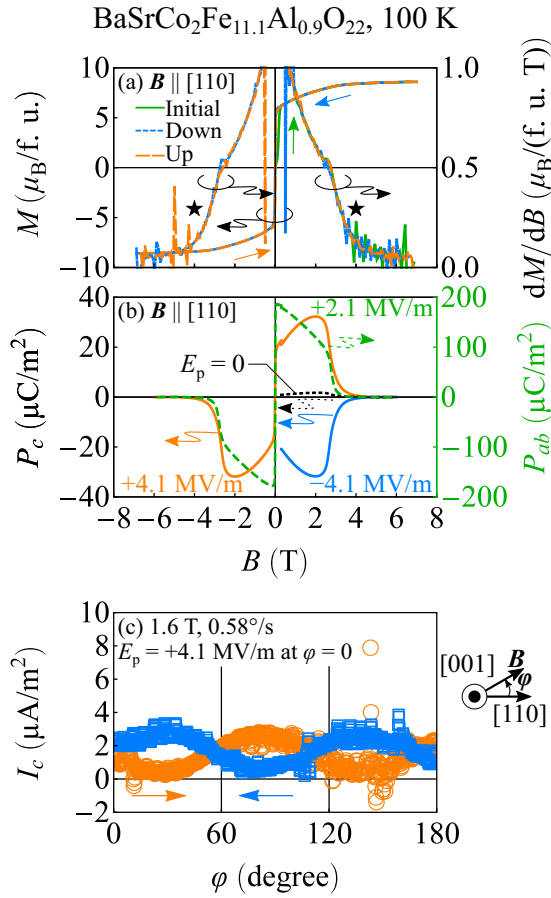
FIG. 2. (a) Isothermal magnetization M and its field derivative measured at 100 K in a magnetic field B along the [110] axis. Black stars indicate the boundaries of ± 3.8 T between the DF and the CFi phases. (b) Electric polarization P_{ab} and P_c measured at 100 K as functions of B along the [110] axis. Before measurement, a poling electric field E_p was applied across the phase transition from the CFi (+6 T) to the DF (+0.3 T). A green dashed line shows the P_{ab} value for $E_p = +2.1$ MV/m. Orange solid, blue solid, and black dotted lines show the P_c data for $E_p = +4.1$ MV/m, -4.1 MV/m, and 0, respectively. (c) Displacement current I_c along the c axis measured at 100 K while rotating B of 1.6 T in the (001) plane at a constant rate of $\pm 0.58°$/s. As shown in the right panel, φ is the azimuth angle of the B direction measured from the [110] axis. Orange circles (blue squares) show data in increasing (decreasing) φ.

Figure 2(c) shows I_c as a function of φ. Here, φ is the azimuth angle of the magnetic field direction measured from the [110] axis in the (001) plane. A large background, which might arise from low electric resistivity, prevents us from estimating P_c. Nevertheless, I_c has a period of 120°, which is consistent with the symmetry-based considerations [Fig. 1(f)]. The periodic behavior cannot be explained by the existence of a possible minor ALC-II phase, since the ↑-↑-↓-↓ sequence of the c components of $\boldsymbol{\mu}_L$ and $\boldsymbol{\mu}_S$, and its consequent P_c would not be affected by the in-plane magnetic field rotation. The observed 120°-period signal is attributable to the DF magnetic order. The nodes of I_c are a little deviated from $60° \times$ (integer), possibly due to some misalignment of a crystalline twofold axis [110] or a (001) plane.
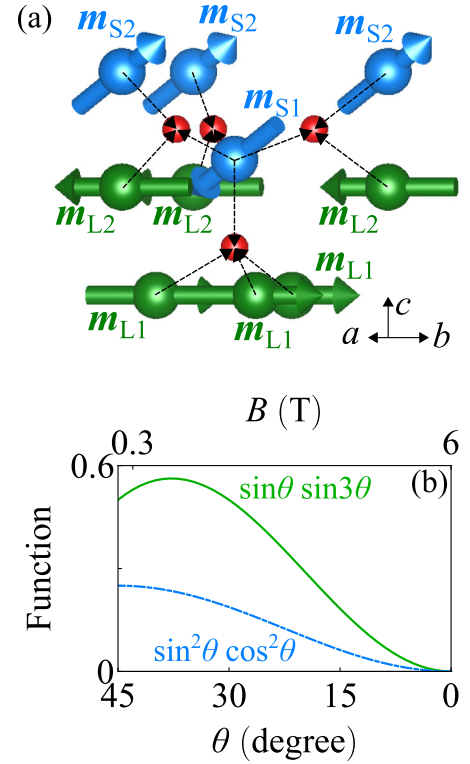

FIG. 3. (a) Arrangement of atoms and magnetic moments around the α boundary. Green (blue) thick arrows indicate the directions of local magnetic moments in the L (S) block, and are parallel or antiparallel to $\boldsymbol{\mu}_L$ ($\boldsymbol{\mu}_S$). (b) Two functions included in the predominant component $p_c^{(1)}$ of the electric dipole moment as a function of θ.

We propose a model to explain the obtained behaviors of P_c. From the viewpoints of symmetry and block approximation, any of the exchange striction, inverse DM interaction, and spin-dependent pd hybridization alone cannot induce P_c in the DF phase. We combine the latter two mechanisms. The spin-dependent pd hybridization mechanism [31] gives the out-of-plane component p_c of the electric dipole moment in a magnetic unit cell (or two primitive unit cells) as

$$p_c = \sum_{u,i} \tilde{p}_{ui} (\hat{\boldsymbol{e}}_{ui} \cdot \boldsymbol{m}_u)^2 (\hat{\boldsymbol{e}}_{ui})_c, \tag{1}$$

which P_c is proportional to. The summation is taken over pairs of neighboring magnetic (u) and oxygen (i) sites. $\tilde{p}_{ui}$ is a constant, $\hat{\boldsymbol{e}}_{ui}$ is the unit vector pointing from a site u to another i, and $\boldsymbol{m}_u$ is a local magnetic moment at the site u. In calculating $\hat{\boldsymbol{e}}_{ui}$, we assume the following displacement $\boldsymbol{d}_i$ of an oxygen ion at a site i by the inverse DM interaction between magnetic moments $\boldsymbol{m}_u$ and $\boldsymbol{m}_v$ around the oxygen ion,

$$\boldsymbol{d}_i = \sum_{u,v} \tilde{d}_{iuv} \hat{\boldsymbol{e}}_{uv} \times (\boldsymbol{m}_u \times \boldsymbol{m}_v), \tag{2}$$

where $\tilde{d}_{iuv}$ is a constant. The displacements are expected only on four boundaries α, β, γ, and δ between the L and S blocks, which are shown in Fig. 1(a). In the figure, oxygen ions subject to the displacements are expressed by red spheres while the others are depicted as black ones.

Figure 3(a) shows a magnified view around the α boundary. The directions of the magnetic moments are expressed as

[20,21]

$$\boldsymbol{m}_{L1}/|\boldsymbol{m}_{L1}| = -\boldsymbol{m}_{L2}/|\boldsymbol{m}_{L2}|$$
$$= \cos(\varphi + \theta_L)\hat{\boldsymbol{e}}_{[110]} + \sin(\varphi + \theta_L)\hat{\boldsymbol{e}}_{[\bar{1}10]}, \quad (3)$$

and

$$\boldsymbol{m}_{S1}/|\boldsymbol{m}_{S1}| = -\boldsymbol{m}_{S2}/|\boldsymbol{m}_{S2}|$$
$$= \cos(\pi - \theta_S)\cos\varphi\,\hat{\boldsymbol{e}}_{[110]} + \cos(\pi - \theta_S)\sin\varphi\,\hat{\boldsymbol{e}}_{[\bar{1}10]}$$
$$+ \sigma\sin(\pi - \theta_S)\hat{\boldsymbol{e}}_{[001]}, \quad (4)$$

where $2\theta_L$ ($2\theta_S$) is the fan angle in the L (S) block ($\theta_L = \theta_S = 0$ corresponds to the CFi structure), $\hat{\boldsymbol{e}}_{[hkl]}$ is the unit vector in the $[hkl]$ direction, and $\sigma\,(= \pm 1)$ distinguishes the sense of the DF. The DF requires that θ_L around the δ boundary should be the same as that around the α boundary, while turned into $-\theta_L$ around the β and γ boundaries. Similarly, $\pi - \theta_S$ should be kept around the β boundary, but turned into $\pi + \theta_S$ around the γ and δ boundaries.

The magnitude $|\boldsymbol{d}_i|$ of the displacement is estimated with the assumption that all oxygen ions are divalent point charges. The inverse DM interaction should displace 16 oxygen ions per magnetic unit cell of the DF. Its volume is $a^2c/\sqrt{3}$, where a and c are lattice constants of Y-type hexaferrites and are roughly 6 and 43 Å, respectively [11,18,21]. The value of P_{ab} is the order of 100 μC/m^2 at most [7,9,17,22]. It corresponds to $|\boldsymbol{d}_i| \sim 1 \times 10^{-4}$ Å, which is much smaller than the bond length between neighboring oxygen and magnetic ions.

The assumptions give the predominant term $p_c^{(1)}$ of p_c as follows [30],

$$p_c^{(1)} = -\frac{3}{2}(A_{L1O1} + A_{L2O2})\sigma\cos(3\varphi)\sin\theta_S\sin 3\theta_L - \frac{3}{2}(A_{S1O2}$$
$$+ A_{S2O2})\sigma\cos(3\varphi)\sin\theta_S\cos^2\theta_S\sin\theta_L. \quad (5)$$

A_{ui} is a constant determined by $\tilde{d}_{iuv}$ and the crystal structure, and is zero when all $\tilde{d}_{iuv}$ are zero. Note that the θ_L, θ_S, and φ dependences of $p_c^{(1)}$ are the same even though various crystal structures and compositions of Y-type hexaferrites produce a difference in A_{ui}. Therefore, Eq. (5) can be applied to BaSrCo$_2$Fe$_{11.1}$Al$_{0.9}$O$_{22}$, whose occupations of Ba/Sr and Co/Fe/Al are not fully identified. Equation (5) explains the 120°-period behavior of P_c and I_c as a function of φ shown in Fig. 2(c). It also contains the coupling between σ and the direction of P_c.

We compare the B dependence of P_c shown in Fig. 2(b) to the model with simplification: The DF phase is homogeneous without any domain walls, and fan angles θ_L and θ_S are both equal to θ. The relation between B and θ is given by the isothermal magnetization as

$$M(B) = M_s\cos\theta. \quad (6)$$

M_s denotes the magnetization of the CFi structure and is estimated from the experimental value at +6 T. The magnetic field of +0.3 T, where the measurement of P_c was started, corresponds to θ of 43°. Figure 3(b) shows $\sin\theta\sin 3\theta$ and $\sin^2\theta\cos^2\theta$, which are parts of Eq. (5). The former takes the extremum in the middle range of θ ($\theta \sim 38°$) and disappears in the CFi state ($\theta = 0$). It qualitatively agrees with the experimental data. The superposition of $\sin\theta\sin 3\theta$ and $\sin^2\theta\cos^2\theta$ does not cancel the nonmonotonic behavior for any set of nonzero $\tilde{d}_{iuv}$ although the latter decreases monotonically to zero.

Since the spin-dependent pd hybridization mechanism reflects the crystalline symmetry, P_c could be induced in U-, X-, and other Y-type hexaferrites belonging to the space group $R\bar{3}m$ in the presence of the magnetic DF, but not in Z-type hexaferrites with the space group $P6_3/mmc$.

In summary, we have revealed that the DF of the Y-type hexaferrite BaSrCo$_2$Fe$_{11.1}$Al$_{0.9}$O$_{22}$ shows both the in-plane P_{ab} and out-of-plane P_c components of magnetically induced electric polarization. P_c has a period of 120° as a function of the in-plane magnetic field direction, as predicted by the crystallographic and magnetic symmetries. The microscopic model employing both the inverse DM interaction and the spin-dependent pd hybridization mechanisms qualitatively explains the observed behaviors of P_c.

[1] J. H. Jung, M. Matsubara, T. Arima, J. P. He, Y. Kaneko, and Y. Tokura, Phys. Rev. Lett. **93**, 037403 (2004).

[2] M. Kubota, T. Arima, Y. Kaneko, J. P. He, X. Z. Yu, and Y. Tokura, Phys. Rev. Lett. **92**, 137401 (2004).

[3] M. Saito, K. Taniguchi, and T.-h. Arima, J. Phys. Soc. Jpn. **77**, 013705 (2008).

[4] I. Kézsmárki, N. Kida, H. Murakawa, S. Bordács, Y. Onose, and Y. Tokura, Phys. Rev. Lett. **106**, 057403 (2011).

[5] S. Toyoda, N. Abe, S. Kimura, Y. H. Matsuda, T. Nomura, A. Ikeda, S. Takeyama, and T. Arima, Phys. Rev. Lett. **115**, 267207 (2015).

[6] Y. Iguchi, Y. Nii, and Y. Onose, Nat. Commun. **8**, 15252 (2017).

[7] T. Kimura, G. Lawes, and A. P. Ramirez, Phys. Rev. Lett. **94**, 137201 (2005).

[8] K. Taniguchi, N. Abe, S. Ohtani, H. Umetsu, and T.-h. Arima, Appl. Phys. Express **1**, 031301 (2008).

[9] S. Ishiwata, Y. Taguchi, H. Murakawa, Y. Onose, and Y. Tokura, Science **319**, 1643 (2008).

[10] Y. S. Chai, S. H. Chun, J. Z. Cong, and K. H. Kim, Phys. Rev. B **98**, 104416 (2018).

[11] P. B. Braun, Philips Res. Rep. **12**, 491 (1957).

[12] J. Smit and H. P. J. Wijn, *Ferrites*, Philips' Technical Library (Cleaver-Hume Press, London, 1959), p. 189.

[13] K. Okumura, T. Ishikura, M. Soda, T. Asaka, H. Nakamura, Y. Wakabayashi, and T. Kimura, Appl. Phys. Lett. **98**, 212504 (2011).

[14] Y. Tokunaga, Y. Kaneko, D. Okuyama, S. Ishiwata, T. Arima, S. Wakimoto, K. Kakurai, Y. Taguchi, and Y. Tokura, Phys. Rev. Lett. **105**, 257201 (2010).

[15] Y. Kitagawa, Y. Hiraoka, T. Honda, T. Ishikura, H. Nakamura, and T. Kimura, Nat. Mater. **9**, 797 (2010).

[16] Y. Yamasaki, S. Miyasaka, Y. Kaneko, J.-P. He, T. Arima, and Y. Tokura, Phys. Rev. Lett. **96**, 207204 (2006).

[17] S. Hirose, K. Haruki, A. Ando, and T. Kimura, Appl. Phys. Lett. **104**, 022907 (2014).

[18] W. Wong-Ng, G. Liu, Y. Yan, K. R. Talley, and J. A. Kaduk, Powder Diffr. **30**, 139 (2015).

[19] V. A. Sizov, R. A. Sizov, and I. I. Yamzin, Zh. Eksp. Teor. Fiz. **53**, 1256 (1967) [Sov. Phys. JETP **26**, 736 (1968)].

[20] N. Momozawa, Y. Yamaguchi, H. Takei, and M. Mita, J. Phys. Soc. Jpn. **54**, 771 (1985).

[21] N. Momozawa and Y. Yamaguchi, J. Phys. Soc. Jpn. **62**, 1292 (1993).

[22] T. Nakajima, Y. Tokunaga, M. Matsuda, S. Dissanayake, J. Fernandez-Baca, K. Kakurai, Y. Taguchi, Y. Tokura, and T.-h. Arima, Phys. Rev. B **94**, 195154 (2016).

[23] S. Ishiwata, D. Okuyama, K. Kakurai, M. Nishi, Y. Taguchi, and Y. Tokura, Phys. Rev. B **81**, 174418 (2010).

[24] H. B. Lee, Y.-S. Song, J.-H. Chung, S. H. Chun, Y. S. Chai, K. H. Kim, M. Reehuis, K. Prokeš, and S. Mat'aš, Phys. Rev. B **83**, 144425 (2011).

[25] S.-P. Shen, X.-Z. Liu, Y.-S. Chai, A. Studer, K. Rule, K. Zhai, L.-Q. Yan, D.-S. Shang, F. Klose, Y.-T. Liu, D.-F. Chen, and Y. Sun, Phys. Rev. B **95**, 094405 (2017).

[26] H. Katsura, N. Nagaosa, and A. V. Balatsky, Phys. Rev. Lett. **95**, 057205 (2005).

[27] I. A. Sergienko and E. Dagotto, Phys. Rev. B **73**, 094434 (2006).

[28] Y. Tokura, S. Seki, and N. Nagaosa, Rep. Prog. Phys. **77**, 076501 (2014).

[29] K. Momma and F. Izumi, J. Appl. Crystallogr. **44**, 1272 (2011).

[30] See Supplemental Material at http://link.aps.org/supplemental/10.1103/PhysRevB.101.100403 for experimental results of $BaSrCo_2Fe_{11.1}Al_{0.9}O_{22}$ at 10 and 200 K, those of $Ba_{0.5}Sr_{1.5}Co_2Fe_{11.1}Al_{0.9}O_{22}$, and calculations in detail.

[31] T.-h. Arima, J. Phys. Soc. Jpn. **76**, 073702 (2007).